

Vortex filament method as a tool for computational visualization of quantum turbulence

Andrew Baggaley

School of Mathematics and Statistics, Glasgow University, UK

Risto Hänninen

O.V. Lounasmaa Laboratory, School of Science, Aalto University, Finland

(Dated: May 13, 2013)

Vortex filament model has become a standard and powerful tool to visualize the motion of quantized vortices in helium superfluids. In this article we present an overview of the method, and highlight its impact in aiding our understanding of quantum turbulence, and in particular superfluid helium. We also present new analysis of the structure and arrangement of quantised vortices. Our results are in agreement with previous studies that under certain conditions vortices form coherent bundles, which allows for classical vortex stretching, giving the quantum turbulence a classical nature.

INTRODUCTION

Turbulence in fluid flows is universal; from galactic scales, generated by supernova explosions, down to an aggressively stirred cup of coffee. There is no debate, turbulence is important, and yet no satisfactory theory exists. Turbulence is built by rotational motions, typically over a wide range of scales, interacting and mediating a transfer of energy to scales where it can be effectively dissipated. The motivation for Kuchemann's famous quote "vortices are the sinews and muscles of fluid motions" is clear. If this is true then quantum turbulence (QT) represents the skeleton of turbulence, and offers a method of attacking the turbulence problem in perhaps its simplest form.

QT is a tangle of discrete, thin vortex filaments, each carrying a fixed circulation. It is typically studied in cryogenically cooled helium [1, 2], and more recently in atomic Bose-Einstein condensates [3]. These are examples of so-called quantum fluids, fluids where certain physical properties cannot be described classically, but depend on quantum mechanics. The quantisation of vorticity is one marked difference between quantum and classical fluids. Another is their two-fluid nature; they consist of a viscous normal fluid component and an inviscid superfluid component coupled by a mutual friction. The relative densities of these components is temperature dependent.

Despite these marked differences, it is now the consensus opinion that QT is capable of exhibiting many of the statistical properties of classical turbulence including the famed Kolmogorov scaling [4]. Hence, QT has the potential to offer new insights into vortex dynamics and the role that they play in the dynamics of turbulence. In addition QT offers many interesting problems in its own right. However quantum turbulence, more so than classical turbulence, suffers from poor visualisation of the flow in experiments, due to the extremely low temperatures involved. Hence numerical methods are necessary to aid

our understanding of the structure of quantised vortices in different forms of turbulence, acting as guide for both experiments and theory. In this article we shall discuss a widely used numerical model of quantum turbulence, the vortex filament model.

VORTEX FILAMENT MODEL

In the vortex filament model (VFM) vortices in the superfluid component are considered as line defects where the phase changes by 2π when going around the core. In helium superfluids the coherence length is typically much smaller than any other characteristic length scale. Therefore the vortex filament model is very suitable and convenient scheme to visualize the vortex dynamics in helium superfluids. Within the vortex filament model the fluid velocity \mathbf{v}_s of the superfluid component is simply determined by the configuration of these quantized vortices and given by Biot-Savart law [5]:

$$\mathbf{v}_s(\mathbf{r}, t) = \frac{\kappa}{4\pi} \int \frac{(\mathbf{s}_1 - \mathbf{r}) \times d\mathbf{s}_1}{|\mathbf{s}_1 - \mathbf{r}|^3}. \quad (1)$$

Here the line integration is along all the vortices and $\kappa = h/m$ is the circulation quantum. For ^4He $m = m_4$ is the bare mass of helium atom (boson). In case ^3He the condensation is made by Cooper pairs, and therefore $m = 2m_3$. The Biot-Savart law expresses the Euler dynamics in integral form by assuming a fluid of constant density [6].

Since the vortices are considered to be thin, the small mass of the vortex core can be neglected, and so at zero temperature vortices move according to the local superfluid velocity. Numerically, the Biot-Savart integral is easily realized by having a sequence of points that describe the vortex. The singularity, when trying to evaluate the integral at some vortex point, \mathbf{s} , can be solved by taking into account that the vortex core size, denoted

by a , is finite [5]:

$$\mathbf{v}_s = \frac{\kappa}{4\pi} \hat{\mathbf{s}}' \times \mathbf{s}'' \ln \left(\frac{2\sqrt{l_+ l_-}}{e^{1/2} a} \right) + \frac{\kappa}{4\pi} \int' \frac{(\mathbf{s}_1 - \mathbf{s}) \times d\mathbf{s}_1}{|\mathbf{s}_1 - \mathbf{s}|^3}. \quad (2)$$

Here l_{\pm} are the lengths of the line segments connected to \mathbf{s} after discretization, and the remaining integral is over the other segments, not connected to \mathbf{s} . Terms $\hat{\mathbf{s}}'$ and \mathbf{s}'' , where the derivation is with respect to arclength, are (unit) tangent and normal at \mathbf{s} , respectively. The first (logarithmic) term on the r.h.s is so-called local term, which typically gives the major contribution to v_s . In the localized induction approximation (LIA) only this term is preserved (possibly adjusting the logarithmic term). This is numerically convenient because the work needed per one time step will be proportional to N which is the number of points used to describe the vortex tangle. Including also the non-local term will require $\mathcal{O}(N^2)$ operations. However, in many cases the non-local term is essential. For example, under rotation, the correct vortex array is only obtained when using the full Biot-Savart integral.

At finite temperatures the motion of quantized vortex is affected by mutual friction, which originates from scattering of quasiparticles from the vortex cores. Typically the vortex motion can be described by using temperature dependent mutual friction parameters α and α' , whose values are well known [7, 8]. Then the velocity of the vortex becomes [5]

$$\mathbf{v}_L = \mathbf{v}_s + \alpha \hat{\mathbf{s}}' \times (\mathbf{v}_n - \mathbf{v}_s) - \alpha' \hat{\mathbf{s}}' \times [\hat{\mathbf{s}}' \times (\mathbf{v}_n - \mathbf{v}_s)]. \quad (3)$$

This is the so-called Schwarz equation which arises by considering the balance of magnus and drag forces acting on the filament. In general the normal fluid velocity, \mathbf{v}_n , should be solved self-consistently, such that vortex motion is allowed to affect the normal fluid. This can be done, as in [9, 10], however the majority of studies in the literature have considered an imposed normal fluid, ignoring an influence of the superfluid on the normal fluid component, which is more achievable numerically. Indeed, this is reasonable approximation in ^3He , where the normal fluid has a viscosity similar to olive oil, and its motion is laminar. However it is not appropriate in ^4He , where the normal component is extremely inviscid. Unfortunately computational limits mean studies with full coupling have, up to now, had limited scope. For example in [10] the simulation was limited to an expanding cloud of turbulence, and no steady state was reached. What is clear is that the next breed of numerical simulations should seek to follow this work and try to understand the dynamics of the fully coupled problem.

The presence of solid walls will alter the vortex motion, since the flow cannot go through the walls. For viscous normal component one typically uses no-slip boundary condition, but for ideal superfluid the boundary condi-

tion is changed to no-flow through boundary, which implies that vortex must meet the smooth wall perpendicularly. For plane boundaries the boundary condition can be satisfied using image vortices, but with more general boundaries one has to solve the Laplace equation for the boundary velocity field potential [5]. This boundary velocity, plus any additional externally induced velocities must generally be included in \mathbf{v}_s and \mathbf{v}_n when determining the vortex motion using Eq. (3). If we are interested purely in homogeneous isotropic turbulence, or flow far from the boundaries then it is typical to work with periodic boundary conditions. These boundaries can also be approximated in the VFM by periodic wrapping; we duplicate the system on surrounding the computational domain with copies of itself, 26 in the case of a periodic cube for example. The contribution of these duplicate filaments is then included in the Biot-Savart integral Eq. (3).

Reconnections

Vortex reconnections are essential in quantum turbulence, allowing the system to be driven to a non-equilibrium steady state [11]. They also change the topology of the tangle [12] and act to transfer energy from three-dimensional hydrodynamic motion to one-dimensional wave motion along the vortices [13]. This is important if we are to understand the decay of QT in the limit of zero temperature, which we discuss briefly towards the end of the article. Moreover, quantum vortex reconnections are not only important phenomena in quantum fluids, but are also relevant to our general understanding of fluid phenomena.

The VFM cannot directly handle vortex reconnections, because reconnections are forbidden by Euler dynamics. Therefore an additional algorithm must be used, which changes the topology of two vortices when they become close to each other, essentially a numerical ‘cut and paste’. Several methods have been introduced to model a reconnection [11, 14–16]. Importantly, a recent analysis [16] has shown that all of these algorithms produce very similar results, at least in case of counter-flow turbulence. Microscopically a single reconnection event has been investigated by using the Gross-Pitaevskii model, which is applicable for Bose-Einstein condensates [17, 18]. A recent numerical simulation of this microscopic model, has shown that the minimum separation between neighbouring vortices are time-asymmetric, like in classical fluids [19]. The VFM, on the other hand, results a more time-symmetric reconnection, where the distance goes mainly like $d \propto \sqrt{\kappa|t - t_{\text{rec}}|}$ where t_{rec} is the reconnection time [18, 20]. The prefactor, however, generally being somewhat larger after the reconnection event. This results from the characteristic curvatures, which are larger after a typical reconnection event [21].

Interestingly the results from the VFM are more compatible with experimental results [22], on the scaling of vortex reconnections. Although reconnections must be introduced ‘by hand’ in the VFM it seems that the model captures the essential physics, at least at scales which can currently be probed experimentally.

Tree-code

A potential drawback of the VFM is the computational time required to perform a simulation which captures the slowly evolving dynamics associated with the largest scale motions. Whilst the LIA is computationally advantageous it has been shown in a number of studies to be unsuitable for studying fully developed quantum turbulence [23]. However, as we have already alluded to, the inclusion of the non-local term in Eq. (2), means the scaling of the velocity computation is $\mathcal{O}(N^2)$. A similar problem was arose in the field of computational astrophysics, where calculations to compute the acceleration due to gravity also required $\mathcal{O}(N^2)$ operations. However, since the pioneering work of Barnes and Hut [24], modern astrophysical and cosmological N-body simulations have made use of tree algorithms to enhance the efficiency of the simulation with a relatively small loss in accuracy [25]. The major advantage of these methods is the $\mathcal{O}(N \log(N))$ scaling which can be achieved. The essence of the method is to retain non-local effects but take advantage of the r^{-2} scaling in Eq. (2). Hence the effect of distant vortices is reasonably small, and an average contribution can be used, if it is computed in a systematic way. A number of recent studies using the VFM have made use of similar tree algorithms [21, 26, 27] to achieve parameter regimes closer to that of actual experiments. It seems clear that tree methods, as in computational astrophysics, will become a standard addition to the VFM.

COUNTERFLOW TURBULENCE

The earliest experimental studies of quantum turbulence came in a series of groundbreaking papers by Vinen in the 1950s [28–31]. In these experiments turbulence was generated by applying a thermal counterflow, where the normal and superfluid components flow in opposite directions. This is easily created by applying a thermal gradient, e.g. by heating the fluid at one end. The most common diagnostic to measure is the vortex line density, $L = \Lambda/V$, where Λ is the total length of the quantised vortices and V is the volume of the system, from this one can compute the typical separation between vortices, the inter vortex spacing $\ell = 1/\sqrt{L}$. This can readily be measured experimentally using second sound [1], and higher harmonics can probe the structure of the tangle.

Numerical simulations have played a crucial role in visualizing the structure of counterflow turbulence, and probing the nature of this unique form of turbulence, indeed it has no classical analogue. Some of the very earliest studies using the vortex filament method were performed by Schwarz [11], however computational limitations meant he was forced to perform an unphysical vortex mixing procedure. A more recent study by Adachi *et al.* [23] made use of modern computational power and studied the dependence of the steady state vortex line density on the heat flux of the counterflow. Within the parameter range of the study, there was a good agreement with experimental results, vindicating the use of the vortex filament method for counterflow turbulence.

Adachi *et al.* also studied the structure of the vortex tangle and in particular the isotropy of the tangle as a function of temperature and heat flux. A more recent study by Baggaley *et al.* [21] probed the structure of the superfluid vortices in thermal counterflow by convolving the tangle with Gaussian kernel to identify any structures in the tangle. In contrast to counterflow, quantum turbulence generated by more conventional methods, such as mechanical stirring, exhibits the famous Kolmogorov scaling, $E(k) \sim k^{-5/3}$ [32]. It is expected [33], and numerically has been observed [34], that this $k^{-5/3}$ scaling is associated with vortex bundling, which may mediate energy transfer in the inertial range. The study of Baggaley

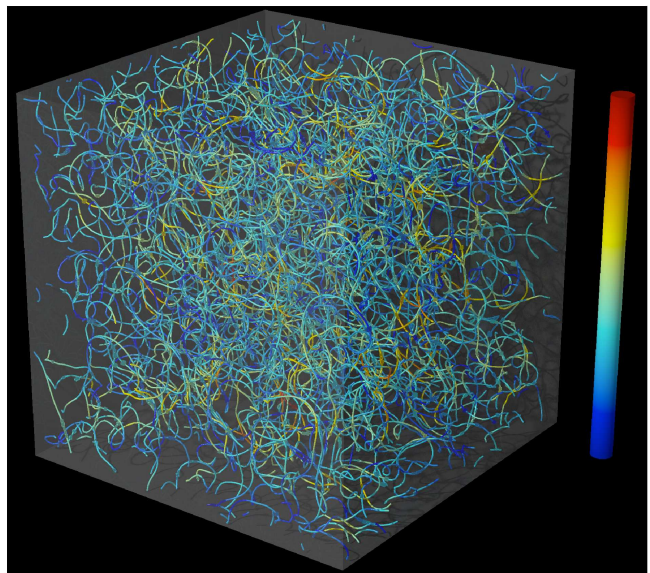


FIG. 1. A visualisation of counterflow turbulence in superfluid ^4He using the VFM in a periodic cube with sides of length 0.1cm. Colored lines represent the position of quantised vortices; the color coding displays the magnitude of the smoothed vorticity, Eq. (5), normalised by the maximum vorticity $\omega = 6.5 \text{ s}^{-1}$ ($\omega_{\text{rms}} = 2.53 \text{ s}^{-1}$). The vortex line density $L = 2.8 \times 10^4 \text{ cm}^{-2}$, and the imposed counterflow velocity $v_{\text{ns}} = 1.25 \text{ cm/s}$.

ley *et al.* [21] showed that this is not the case in counterflow, with the tangle being relatively featureless and consisting of random closed loops which leads to a featureless energy spectrum, without motion of many scales, which is the hallmark of classical turbulence. Figure 1 illustrates the relatively unstructured tangle of vortices from a numerical simulation of counterflow turbulence, here we evolve the vortices according to Eq. (3) with $\alpha = 0.206$, $\alpha' = 0.00834$ ($T=1.9K$), $\mathbf{v}_n = (1.25, 0, 0)$ cm/s; further technical details can be found in [21].

Visualisation of the counterflow turbulence, and detailed analysis of the nature of the flow the vortices induce, also have direct consequences for analytic theories of quantum turbulence. For example, Nemirovskii *et al.* [35] considered the energy spectrum of the velocity field induced by a random set of quantised vortex rings, the analytic spectrum they predicted is quantitatively similar to the energy spectrum obtained numerically by Baggaley *et al.* [21].

A particularly striking example, where the power to visualise quantum turbulence has helped to answer an apparent puzzle is the anomalous decay of counterflow turbulence. Experimentally it was observed that after switching off the heater the density of quantised vortices decreased in time, as to be expected. However in the early stages of the decay the process was very slow, and it was even observed that the vortex line density could increase, after turning off the drive. An explanation was provided in [36] where they showed, using the VFM, that the tangle created by counterflow is strongly polarized. However, after switching off the drive, the vortex lines depolarise. As experimental measurements are based on second sound, this depolarisation creates an apparent increase in the measured vortex line density, which is purely an artefact of the measurement process, a truly beautiful result.

However, there are still a number of open and important questions related to the problem of counterflow turbulence. For example there are a number of different turbulent states in counterflow [37], what is the nature of these different regimes; in particular, is the normal fluid turbulent. Experimentally it is also possible to create pure superflow, where the normal fluid is held static. Whilst initially this may seem purely a Galilean transform of the problem of counterflow, results [38] indicate differences between the two states. As has already demonstrated, the VFM should prove an important tool to help answer these questions.

TWO-FLUID TURBULENCE

Whilst thermal counterflow is a unique form of turbulence, possible only in quantum fluids, one of the main motivations behind the study of QT is in the so-called semi-classical regime, where the statistical properties of

the turbulence show tantalising similarities with normal viscous fluids. In particular this regime has been the focus of a number of experimental studies [32, 39], where the classical Kolmogorov energy spectrum and higher order statistical measures such as structure functions, show agreement with classical studies. This result was also reproduced using the VFM, at 0K, by Araki *et al.* [40] by studying the evolution of quantised vortices arranged as the classical Taylor-Green vortex.

In addition the VFM has played an important role in allowing us to visualise the structure of the quantised vortices, under the influence of a turbulent normal fluid. A particularly influential study was made by Morris *et al.* [41] where a full numerical simulation of the Navier-Stokes equation was coupled to the VFM. They observed a locking between vortices in the superfluid component and intense vortical regions in the normal component. This built upon an earlier study by Kivotides [42] where a similar result was obtained, but for a frozen normal fluid velocity field, generate by a turbulent tangle of classical vortex filaments.

In a more recent paper Kivotides [26] considered the effect of coherent superfluid vortex bundles on an initially stationary normal fluid. Computations were performed using the VFM coupled to the Navier-Stokes equation, with mutual friction accounted for as a forcing term in the Navier-Stokes. He showed that the induced normal-fluid vorticity acquired a similar morphology to the structures in the superfluid fraction, and argued the dynamics of fully developed, two fluid turbulence was depended on interactions of coherent vortical structures in the two components.

Indeed, in classical turbulence these nonlinear structures, vortical ‘worms’, appear to play a crucial role in the dynamics of the inertial range [43]. In a more recent study Baggaley *et al.* [34] developed a procedure to decompose the vortex tangle into a coherent ‘bundled’ component and a random component. Algorithmically this was achieved by convolving the vortex tangle with a cubic spline

$$\omega(\mathbf{s}_i) = \kappa \sum_{j=1}^N \mathbf{s}'_j W(r_{ij}, h) ds_j, \quad (4)$$

where $r_{ij} = |\mathbf{s}_i - \mathbf{s}_j|$, $ds_j = |\mathbf{s}_{j+1} - \mathbf{s}_j|$, $W(r, h) = g(r/h)/(\pi h^3)$, h is a characteristic length scale, and

$$g(q) = \begin{cases} 1 - \frac{3}{2}q^2 + \frac{3}{4}q^3, & 0 \leq q < 1; \\ \frac{1}{4}(2-q)^3, & 1 \leq q < 2; \\ 0, & q \geq 2. \end{cases} \quad (5)$$

It is appropriate to take h equal to the inter-vortex spacing, this effectively smearing the quantised vorticity to create a continuous vector field in space. Thus at any point an effective ‘vorticity’ can be defined, in particular vortex points with a high vorticity (above a threshold

level based on the root mean squared vorticity) were categorised as part of the coherent component. Analysis of these two components showed that it is the vortex bundles which create the inertial range of the turbulence and the random component is simply advected in the manner of a passive tracer.

In the next section we shall consider the rotating quantum fluids where we shall apply this smoothing algorithm to identify transient coherent structures which appear in the system.

SUPERFLUIDS UNDER ROTATION

Rotating fluids are ubiquitous in the universe, and so the study of classical fluids under rotation forms a vast topic in its own right. Within viscous fluids several different flow profiles have been observed, depending on external conditions etc. In helium superfluids rotation has actively been used to investigate the vortex dynamics. The steady state under constant rotation is typically a vortex array that mimics the normal fluid profile. However, before this steady state is reached, turbulence may appear. This is especially true at low temperatures when the mutual friction is low [49, 50, 53]. The onset and the initialization of turbulence has been attributed to the instability that originates from interaction of the vortex with the container walls [51–53].

Vortex Front

In superfluid $^3\text{He-B}$ the vortex core size is large enough that the container surfaces can be prepared to be suitably smooth, and the critical velocity for vortex nucleation due to surface roughness can be adjusted large enough, to provide a vortex free rotation (so-called Landau state) even at relatively large rotation velocities. Now, if vorticity is introduced, for example using the Kelvin-Helmholtz instability of the AB-phase boundary [54], a propagating vortex front can be generated. The front separates a vortex free region from a vortex array as illustrated in Fig. 2. At low enough temperatures the front becomes turbulent and the vortex array behind the front becomes twisted, eventually relaxing to straight vortices [55]. The propagation velocity of the front is proportional to the dissipation. At the lowest observable temperatures ($T \sim 0.15T_c$) the coupling with the normal fluid almost vanishes, but the energy dissipation still remains finite, orders of magnitudes larger than one would obtain from the laminar prediction [56]. However, the dissipation of angular momentum remains weak, which is seen from the rotation velocity of the vortex array behind the front. At lowest temperatures this rotation velocity drops much below the rotation velocity of the cylindrical cell [57]. In a way, the vortex motion decouples from the external refer-

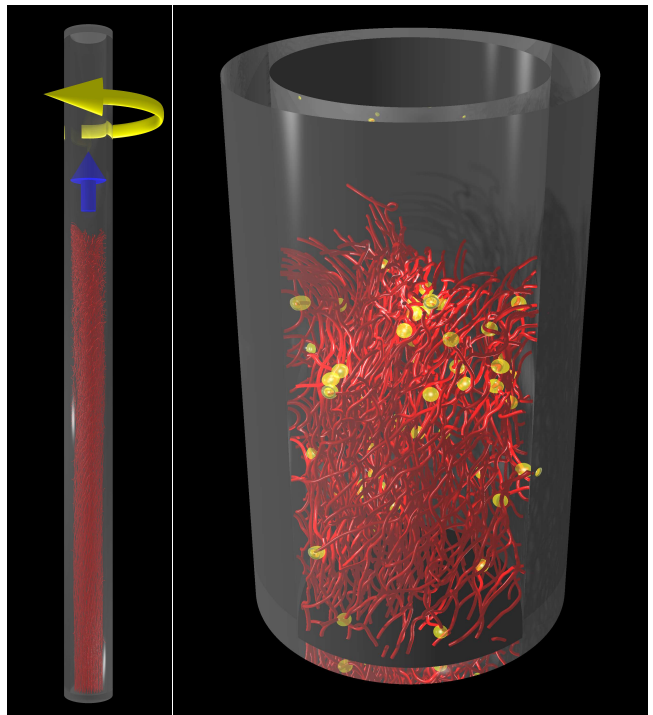


FIG. 2. (left) Propagating vortex front in $^3\text{He-B}$ at $T = 0.30T_c$ when the cylinder radius $R = 1.5$ mm and the rotation velocity $\Omega = 1.0$ rad/s (indicated by the yellow arrow). (right) Vortex structures in the front region where the reconnection events have been highlighted by yellow flashes.

ence frame of the rotating cylinder. All of these features are also observed in vortex filament simulations [56, 57]. Most recently the VFM helped to develop a simple model, which explains the observed behavior [58].

The filament model can also be used to visualize the vortex front in more detail, since experimentally the measurements are performed using NMR imaging that is only sensitive to the average counterflow in the vicinity of the coil, which does not provide information about individual vortex motion. Currently numerical resolution limits the lowest temperatures that can be simulated, since as the temperature is lowered, smaller and smaller scale structures appear, which dominate the mutual friction dissipation. Therefore, the zero temperature limit requires either much better resolution, or inclusion of novel dissipation mechanisms, other than mutual friction. In case of $^3\text{He-B}$, for example, one could include the vortex core dissipation introduced by Silaev [59].

The largest discrepancy between simulations and experiments is the initialization of the front. Experimentally the front can be initialized at low temperatures by few seed vortices that interact and soon generate a large number of vortices during a turbulent burst. These vortices then expand and form a front. However in numerical simulations with the VFM, the initialization of the front must be done using a large number of vortices. Taking

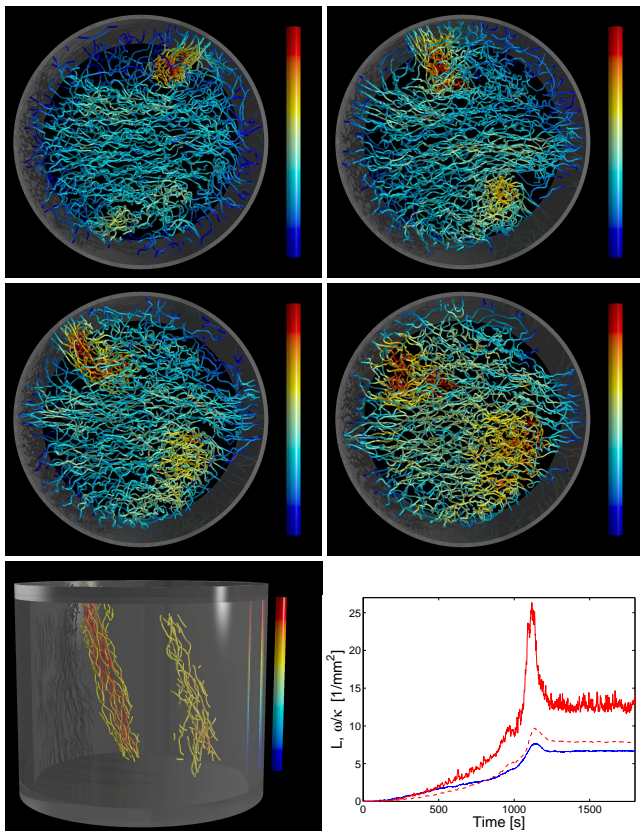


FIG. 3. Coherent structures that appear in a tilted cylinder during the spin-up of the superfluid component. Superfluid $^3\text{He-B}$ at $T=0$ with $R = 3$ mm, $L = 5$ mm, $\Omega = 0.25$ rad/s, and tilt angle of 30 degrees. The configurations are shown at times $t = 1100$ (top left), 1130 (top right), 1140 (center left), and 1150 (center right) seconds and the color coding illustrates the relative amplitude of the smoothed vorticity. The bottom left panel illustrates the coherent structures at $t = 1140$ s, where only the coherent part with $\omega > 1.4\omega_{\text{rms}}$ is plotted. The bottom right panel illustrates the temporal evolution of the vortex line density, L (lowest, blue solid line), together with the r.m.s. (dashed, red line) and maximum vorticity (upper, red solid line).

into account surface friction or pinning might remove this discrepancy.

Coherent structures

In this article, we have applied the cubic spline smoothing, Eq. (4), on the vortex structures that appear during the spin-up (by suddenly increasing the rotation velocity) of the superfluid component, in the case of a cylinder that is strongly tilted with respect to the rotation axis [60]. These simulations show that coherent vortex structures (vortex bundles) appear, at least at low temperatures. This is illustrated in Fig. 3, where the initial configuration of a single vortex loop expands due to the applied flow and generates a very polarized vortex tangle, which

eventually approximates solid body rotation. We have now identified the vortex clusters, which appear slightly before the configuration reaches the steady state. They appear during the “overshoot” period and quickly merge to the background vorticity. It is also interesting to note that the steady state that approximately mimics the solid body rotation is reached even at zero temperature, where the mutual friction coefficients are set to zero. Naturally, there exists some small numerical dissipation. A somewhat more peculiar feature from these simulations is that the steady state is not fully static, even at somewhat higher temperatures. This might be because the boundary induced velocity in these simulations is only solved approximately (by using image vortices) [60]. Alternatively, the simulations are perhaps stuck in some other local energy minimum, which is not the true minimum.

DECAY OF QUANTUM TURBULENCE

Spin-down

The decay of quantized vortices at low temperatures after a sudden stop of rotation (spin-down) has been analyzed in several experiments, both in superfluid $^3\text{He-B}$ and $^4\text{He-II}$. The $^3\text{He-B}$ experiments conducted in cylindrical container show a laminar type decay, where the vorticity typically decays as $1/t$ [53, 62]. In contrast, the experiments in $^4\text{He-II}$ using a cubical container show a turbulent decay, where vorticity decreases faster, proportional to $t^{-3/2}$, and is preceded by a strong overshoot, just after stopping the rotation [50, 61]. Even if the stronger pinning in $^4\text{He-II}$ may favor turbulence over laminar behavior, the recent simulation which used smooth walls, where pinning is neglected, show that the geometry has a strong effect on the decay behavior at low temperatures. Simulations conducted in a sphere, or in a cylinder where the cylinder axis is close to the initial rotation axis, show a laminar decay where the vortices remain highly polarized. In contrast, calculations performed in a cubical geometry, or if the tilt angle for the cylinder is large, indicate turbulent decay [53, 62].

In cylindrically symmetric containers, the decay of vorticity is observed to occur in a laminar fashion, which can be explained by using the Euler equation for inviscid and incompressible flow in uniform rotation. If the initial vorticity corresponds to an equilibrium state given by the initial rotation, Ω_0 , and if the rotation is set to rest, then the solution for radial part of the two-dimensional motion of the vorticity $\Omega_s(t)$ is given by $\Omega_s = \Omega_0/(1 + t/\tau)$ [53, 63]. The decay time is simply given by the mutual friction as $\tau = 1/(2\alpha\Omega_0)$. This appropriately models the vorticity in the bulk, where the polarization is near 100% and the coarse-grained vorticity is spatially homogeneous. In simulations the dissipation of vorticity (vortex line length) occurs within a thin boundary

layer whose thickness increases as temperature (mutual friction dissipation) decreases [53]. What happens in the zero temperature limit is still a somewhat open question. Presumably, the thickness of the boundary layer increases as $T \rightarrow 0$ so that the laminar decay becomes impossible with vanishing mutual friction.

In cubical containers, or if the cylindrical symmetry is broken, *e.g.* by strongly tilting the cylinder, the decay shows turbulent behavior, even if the polarization remains non-zero (reflecting the long-surviving vortex array). After an initial overshoot, the decay is faster than in the laminar case. Reconnections are here distributed more evenly in the bulk, indicating turbulence in the whole volume. In addition to the vortex array, the most visible indication of coherent structures are the helical distortions of this array. This is illustrated in Fig. 4 where we have applied the vortex smoothing process on recent spin-down simulations conducted in a cube. These coherent oscillations of the vortex array appear shortly after the rotation is stopped and might be related to the lowest resonant modes. Because the smoothed vorticity resulting from the vortex array is rather uniform and the fluctuations from this level are quite small, the numerical identification of additional structures, if they exist, becomes difficult. However, the faster decay and the apparent absence of different size coherent structures, typical for Kolmogorov turbulence, might indicate that the decay of type $t^{-3/2}$ is more general than expected.

The decay of a random tangle

Of course the study of turbulent decay is not limited to rotating cases, indeed the decay of homogeneous isotropic turbulence is an important field of research. Here we focus on the decay of QT in the limit of zero temperature. Towards the end of the article we shall focus on the physical mechanisms of energy dissipation, here we shall limit ourself to the scaling of the decay, as this is also readily measured experimentally. Experiments in helium have revealed two distinct regimes of decay of a random tangle of quantised vortices, by monitoring the vortex line density L in time. These are the so-called ultraquantum decay, characterised by $L \sim t^{-1}$, and semi-classical, $L \sim t^{-3/2}$, regimes. Perhaps the most striking example of these two regimes came in a study by Walmsley and Golov [44]. By injecting negative ions into superfluid ^4He , in the zero-temperature limit, they observed the two regimes of turbulence decay. The negative ions (electron bubbles) generated vortex rings, which subsequently interacted, forming a turbulent vortex tangle. After switching of the ion injection the turbulence would then decay. If the injection time was short they observed the ultra quantum regime, whereas for a longer injection time semi-classical behaviour was apparent.

Walmsley and Golov argued that the second regime is

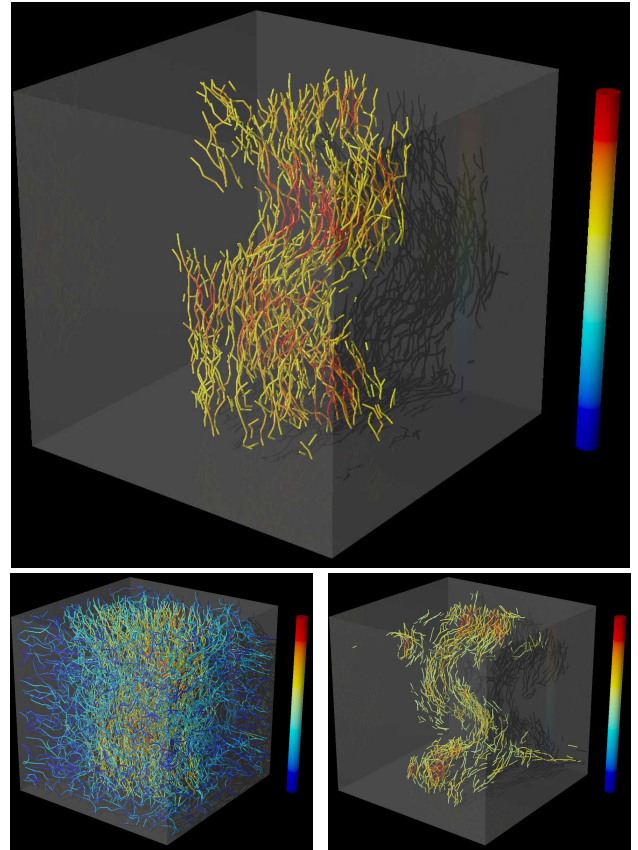


FIG. 4. Decay of vorticity in superfluid $^3\text{He-B}$ after a sudden stop of rotation from $\Omega_0 = 0.5$ rad/s. Initial state inside the cube (side 6 mm) was a steady state vortex array, with a small tilt to break the symmetry. The upper figure illustrates the coherent vortex part ($\omega > 1.4\omega_{\text{rms}}$) at $T = 0.20T_c$ with $t = 87$ s. The bottom left figure illustrates the full vortex configuration with $\omega_{\text{rms}} = 9.23 \text{ s}^{-1}$ and $\omega_{\text{max}} = 21.05 \text{ s}^{-1}$. The bottom right figures illustrates again the coherent part, but now at slightly higher temperature, $T = 0.22T_c$, and $t = 64$ s. Here $\omega_{\text{rms}} = 10.90 \text{ s}^{-1}$ and $\omega_{\text{max}} = 29.23 \text{ s}^{-1}$. Colouring of the lines shows the smoothed vorticity, normalised by the maximum smoothed vorticity.

associated with the classical Kolmogorov spectrum at low wave numbers, whereas the ultraquantum regime was due to the decay of an unstructured tangle with no dominant large scale flow. Both regimes were also observed in $^3\text{He-B}$ by Bradley *et al.* [45], by forcing turbulence with a vibrating grid.

A numerical study, using the VFM, by Fujiyama *et al.* [46] showed some evidence that a tangle generated by loop injection could exhibit semi-classical behaviour and decay like $L \sim t^{-3/2}$. A more comprehensive study by Baggaley *et al.* [47] drew inspiration from the experiment of Walmsley and Golov, and considered both short and long injection time. This study reproduced both the ultraquantum and the semi-classical regimes, and by examining both the curvature of the filaments and the

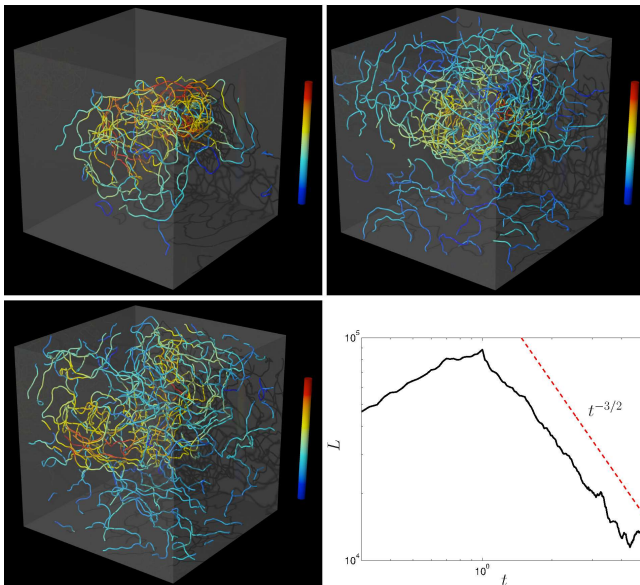


FIG. 5. Decay of semi-classical turbulence in superfluid ^4He , the vortex configurations are plotted at $t = 0.1\text{ s}$ (top-left), $t = 0.75\text{ s}$ (top-right) and $t = 1.1\text{ s}$ (bottom-left), the colouring of the lines shows the smoothed vorticity, normalised by the maximum smoothed vorticity ($\omega_{\text{max}} = 16.31, 37.7$ and 29.3 s^{-1} respectively.) The shaded box shows the periodic domain of the simulation, a cube of side 0.03 cm . The corresponding vortex line densities are $4.1 \times 10^4, 7.8 \times 10^4$ and $7.5 \times 10^4\text{ cm}^{-2}$; The evolution of the vortex line density and the semi-classical scaling is displayed in the bottom-right panel.

superfluid energy spectrum, confirmed the hypothesis of Walmsley and Golov. In the semi-classical regime the initial energy distribution was shifted to large scales, and a Kolmogorov spectrum was formed. If we now revisit the structure of the tangle in the semi-classical simulation, and perform the convolution with a cubic spline, Eq. (5), then we can see coherent bundling of the vortices, potentially due to the strong anisotropy in the loop injection, see Fig. 5. In the ultraquantum case, as the injection time was short the spectrum decays without this energy transfer, and very little energy is in the large scale motions.

MOTION OF TRACER PARTICLES

In classical fluid mechanics the use of tracer particles and the technique of particle image velocimetry (PIV) are standard techniques to visualise experimental flows [68, 69]. In helium superfluids the low temperatures, and the low viscosity of ^4He , strongly limit the usability of different tracer materials. However, in 2005 Zhang *et al.* managed to visualize the thermal counterflow around a cylinder by using polymer particles. Soon after, Bewley *et al.* [71] used small micron-size hydrogen particles to

directly visualize quantized vortices, and vortex reconstructions [22].

Generally the two fluid nature of helium superfluids complicates the analysis of the tracer particles. The particles may be trapped/affected by the vortex lines or they may simply follow the normal fluid or trace the total mass current. All this depends on temperature, particle size, and fluid velocity as analyzed by Poole *et al.* [72]. They also concluded that the vortex trapping is a rather common phenomena, appearing *e.g.* in counterflow turbulence. Kivotides *et al.* [73] have combined the vortex filament simulations with the equation of motion derived for a spherical particle in Refs. [74, 75]. These self-consistent calculations have been used in a number of studies, to estimate the trapping probability and typical trajectories of tracer particles at different temperatures [76–79]. One outcome of these simulations is that the trapping becomes more probable at higher temperatures.

Even without self-consistent calculations for the tracer particles, simulations have already been used to explain the non-classical (non-Gaussian) velocity distributions observed in counterflow experiments by Paoletti *et al.* [80]. White *et al.* [81], by using the GP equation, and Adachi & Tsubota [82] together with Baggaley & Barenghi [27], by using the filament model, illustrated that the velocity distribution takes the form $Pr(v) \propto v^{-3}$. This simply results from the $1/r$ velocity field induced by a quantized vortex. The contradiction with experiments by Salort *et al.* [83], where the velocity statistics was observed to be classical, was explained by Baggaley & Barenghi [84], who noticed that on scales larger than inter-vortex distance the quantum turbulence exhibits again quasiclassical behaviour.

VIBRATING OBJECTS

A common method to generate turbulence in helium superfluids is to use vibrating objects, see *e.g.* Refs. [64, 65] and references therein. A vibrating wire, sphere, grid, or a quartz tuning fork generates a vortex tangle around it, which can be experimentally observed by measuring the extra dissipation. At small drives the measured damping force is linear with respect to oscillating velocity and can be explained by ballistic phonon scattering for $^4\text{He-II}$. For larger drive forces a nonlinear turbulent drag can be observed which is attributed to turbulence in the superfluid component. The drag force also takes a similar form to that seen in classical viscous fluids, with the exception that the force is not simply proportional to v^2 but rather to $(v^2 - v_0^2)$ reflecting that the turbulence only occurs above some critical velocity v_c [65, 85]. At velocities slightly above v_c one typically observes hysteresis and switching phenomena between laminar and turbulent states [86–88].

A turbulent burst around a vibrating sphere at large

enough velocities was first observed in vortex filament simulations by Hänninen *et al.* [64]. Those simulations did not reach a steady state, which was later obtained in simulations by Nakatsuji *et al.* [66]. They additionally analyzed the size and the direction distribution of emitted vortex loops that escape from the vortex tangle around the sphere. The simulations by Goto *et al.* [67] verified the experimental observation that turbulence around a vibrating wire can be triggered and kept alive by simply injecting small vortex loops from another wire that is in turbulent state. Currently the simulations related to vibrating objects lack a fully self-consistent treatment that takes into account the force experienced by the vibrating object due to quantized vortices. In the future, these kind of simulations might give us more insight what is really happening around wires and grids and they might explain also the switching phenomena between the laminar and turbulent states.

KELVIN-WAVE CASCADE

If the temperature is relatively large (greater than 1K in ^4He), turbulent kinetic energy contained in the superfluid component is transferred by mutual friction into the normal fluid, and subsequently into heat via viscous heating. A constant supply of energy (continuous stirring for example) is needed to maintain the intensity of the turbulence. At very low temperatures the normal fluid is negligible, but despite the absence of mutual friction, the turbulence still decays [44, 90]. The Kelvin-wave cascade (KWC) [13] is perhaps the most important of the proposed mechanisms to explain this surprising effect.

Kelvin waves are a classical phenomena [89], a rotating sinusoidal or helical perturbation of the core of a concentrated vortex filament. The KWC is the process in which the nonlinear interaction of Kelvin waves create higher frequency modes. At very high frequency (where the wavelength is atomic scale) sound is efficiently radiated away (phonon emission) by rapidly rotating vortices. Hence in contrast to classical turbulence, where the energy sink is viscous, in QT the energy sink is acoustic. Crucially Kelvin waves are easily generated in QT, vortex reconnections typically create a high curvature cusp [91], which acts as a mechanism to transfer energy from three dimensional hydrodynamic turbulence, to one-dimensional wave turbulence along the vortex filaments.

It is currently believed that there are two regimes in the KWC, one corresponding to large amplitude waves, and another to a low amplitude, weakly nonlinear regime, where the theory of wave turbulence can be applied [92]. It is in this weakly nonlinear regime where the VFM can play a crucial role in distinguishing between a number of proposed theories [93–95]. The key prediction of each theory is in the spectrum of the kelvon occupation

numbers, with each giving different power-law scalings, $n_k \sim k^{-\alpha}$. In particular Kozik and Svistunov (KS) [93] proposed $\alpha = 17/5$, L’vov *et al.* [94] claimed the KS spectrum was invalid, due to the assumption of locality of interactions, and proposed a nonlocal theory which predicted $\alpha = 11/3$. Whilst it is not simply the spectrum of n_k which distinguishes these two theories, this is perhaps the easiest statistic to compute with the VFM, as n_k is related to the Kelvin-wave amplitudes. However, the fact that these exponents are so similar, clearly provides a huge computational challenge, if one is to provide strong evidence for either theory.

Vinen *et al.* [96] considered a rectilinear vortex in a periodic domain, KWs were excited with an external superflow, which forced a single planar KW mode. They observed a spectrum consistent with $\alpha = 3$, although visual inspection shows a slightly steeper spectrum. Later Kozik & Svistunov [97] developed a scale-separation scheme, significantly reducing the cost of a full Biot-Savart simulation, and argued that their simulation showed strong evidence of the $n_k \sim k^{-17/5}$ spectrum, in agreement with their theoretical predictions. Baggaley & Barenghi [98] considered the KWC driven by reconnecting vortex rings and showed a spectrum consistent with rival theories, $\alpha > 3$, however a more refined prediction was not possible. The problem of numerical approaches to the KWC was crystallised in a recent article by Hänninen & Hietala [99]. They showed that erroneous numerical methods can result in a spectrum that is totally incorrect, but still very close to the spectrum predicted theoretically. Indeed we would argue that no convincing evidence for either theory has yet been demonstrated using the VFM, and this remains an open and challenging problem.

Bottleneck?

Whilst much attention has focused on the KWC, perhaps of more importance, in particular to experimental interpretation, is how the 1D KWC matches to the 3D hydrodynamic energy spectrum. Once again rival theories have been proposed by the groups of Kozik & Svistunov and L’vov and collaborators. To summarise the situation briefly, L’vov *et al.* predict a bottleneck in energy, which is required for continuity in the energy flux at the crossover scale, and so one should expect an increase in the vortex line density, at scales of the order of the intervortex spacing, ℓ . This is countered by KS [100], who argued for a number of different reconnection regimes between the Kolmogorov and Kelvin wave spectra, which does not create such a bottleneck. Again this is an open and important question, which has yet to be studied in detail using the VFM. The large range of scales involved means that new numerical approaches, such as the tree-code discussed earlier, will be vital to make any

progress.

CONCLUSIONS

To summarise we hope that the reader will agree that the VFM has proven to be a valuable tool in the study of superfluid turbulence, and quantised vortex dynamics. Of course despite some of the success stories we have described here, there is still much work to be done. Much attention in the literature has focused on the Kelvin-wave cascade, and perhaps rightly so. However other decay mechanisms, such as loop emission due to vortex reconnections [101], warrant further investigation. Indeed they could play an important role in the decay of the unstructured ‘Vinen’ tangle.

The field itself will of course be driven by experimental studies, and it is an exciting time with many new investigations planned in the near future. However the role of the VFM in aiding to analyse and interpret this experimental data, and test, refine and motivate analytic theories remains important.

However, superfluid turbulence is not just found in the laboratory. There are important astrophysical applications. Current theory strongly suggests that the outer core of neutron stars consists of neutrons in a superfluid state. Due to incredibly rapid rotation we would expect this superfluid to be threaded by quantised vortices, pinned to the solid outer crust. Interesting phenomena, such as rapid changes in the rotation rate, are observed and thought to be related to the behaviour of the quantised vortices [102]. Such a system could be reasonably modelled with the VFM and it remains an interesting problem awaiting such an investigation.

This work is supported by the EU 7th Framework Programme (FP7/2007-2013, grant 228464 Microkelvin). R.H. acknowledge financial support from the Academy of Finland. R.H would also like to thank N. Hietala for useful discussions and CSC - IT Center for Science Ltd for the allocation of computational resources.

[1] Donnelly RJ (1991) *Quantized Vortices in Helium II* (Cambridge University Press, Cambridge).
 [2] *Quantized Vortex Dynamics And Superfluid Turbulence*, Springer’s Lecture Notes in Physics **571**, eds Barenghi CF, Donnelly RJ, Vinen WF (2001).
 [3] Henn EAL, Seman JA, Roati G, Magalhães KMF, Bagnato VS (2009) Emergence of turbulence in an oscillating Bose-Einstein condensate. *Phys Rev Lett* 103:045301.
 [4] Vinen WF, Niemela JJ (2002) Quantum turbulence. *J Low Temp Phys* 128:167-231.
 [5] Schwarz KW (1985) Three-dimensional vortex dynamics in superfluid ^4He : Line-line and line-boundary interactions. *Phys Rev B* 31:5782-5804.

[6] Saffman PG (1992) *Vortex Dynamics*, (Cambridge University Press, Cambridge).
 [7] Bevan TDC et al. (1997) Vortex mutual friction in superfluid ^3He . *J Low Temp Phys*, 109:423-459.
 [8] Donnelly RJ, Barenghi CF (1998) The observed properties of liquid helium at saturated vapour. *J Phys Chem Ref Data* 27:1217.
 [9] Kivotides D, Barenghi CF, Samuels DC (2000) Triple vortex ring structure in superfluid helium. *Science* 290:777.
 [10] Kivotides D (2011) Spreading of superfluid vorticity clouds in normal-fluid turbulence. *J Fluid Mech* 668:58-75.
 [11] Schwarz KW (1988) Three-dimensional vortex dynamics in superfluid ^4He : Homogeneous superfluid turbulence. *Phys Rev B* 38:2398-2417.
 [12] Poole DR, Scofield H, Barenghi CF, Samuels DC (2003) Geometry and topology of superfluid turbulence. *J Low Temp Phys*, 132:97-117.
 [13] Svistunov BV (1995) Superfluid turbulence in the low-temperature limit. *Phys Rev B* 52:3647-3653.
 [14] Kondaurova L, Nemirovskii SK (2008) Numerical simulations of superfluid turbulence under periodic conditions. *J Low Temp Phys* 150:415-419.
 [15] Tsubota M, Araki T, Nemirovskii SK (2000) Dynamics of vortex tangle without mutual friction in superfluid ^4He . *Phys Rev B* 62:11751-11762.
 [16] Baggaley A W (2012) The sensitivity of the vortex filament method to different reconnection models. *J Low Temp Phys* 168:18-30.
 [17] Koplik J, and Levine H (1993) Vortex reconnection in superfluid helium. *Phys Rev Lett* 71:1375-1378.
 [18] Zuccher S, Caliori M, Baggaley AW, Barenghi CF (2012) Quantum vortex reconnections. *Phys Fluids* 24:125108.
 [19] Hussain F, Duraisamy K (2011) Mechanics of viscous vortex reconnection. *Phys Fluids* 23:021701.
 [20] de Waele ATAM, Aarts RGKM (1994) Route to vortex reconnection. *Phys Rev Lett* 72:482-485.
 [21] Baggaley AW, Sherwin LK, Barenghi CF, Sergeev YA (2012) Thermally and mechanically driven quantum turbulence in helium II. *Phys Rev B* 86:104501.
 [22] Paoletti MS, Fisher ME, Lathrop DP (2010) Reconnection dynamics for quantized vortices. *Physica D* 239:1367-1377.
 [23] Adachi H, Fujiyama S, Tsubota M (2010) Steady-state counterflow quantum turbulence: Simulations of the vortex filaments using the full Biot-Savart law. *Phys Rev B* 81:104511.
 [24] Barnes J, Hut P (1986) A hierarchical $O(N \log N)$ force-calculation algorithm. *Nature* 324:446-449.
 [25] Bertschinger E (1998) Simulations of structure formation in the universe. *Ann Review Astronomy and Astrophysics* 36:599-654.
 [26] Kivotides D (2007) Relaxation of superfluid vortex bundles via energy transfer to the normal fluid. *Phys Rev B* 76:054503.
 [27] Baggaley AW, Barenghi CF (2011) Vortex-density fluctuations in quantum turbulence. *Phys Rev B* 84:020504.
 [28] Vinen WF (1957) Mutual friction in a heat current in liquid helium II. I. Experiments on steady heat currents. *Proc R Soc Lond A* 240:114-127.
 [29] Vinen WF (1957) Mutual friction in a heat current in liquid helium II. II. Experiments on transient. *Proc R*

- Soc Lond A* 240:128-143.
- [30] Vinen WF (1957) Mutual friction in a heat current in liquid helium II. III. Theory of the mutual friction. *Proc R Soc Lond A* 242:493-515.
 - [31] Vinen WF (1958) Mutual friction in a heat current in liquid helium II. IV. Critical heat currents in wide channels. *Proc R Soc Lond A* 243:400-413.
 - [32] Maurer J, Tabeling P (1998) Local investigation of superfluid turbulence. *Europhys Lett* 43:29-34.
 - [33] L'vov VS, Nazarenko SV, Rudenko O (2007), Bottleneck crossover between classical and quantum superfluid turbulence. *Phys Rev B* 76:024520.
 - [34] Baggaley AW, Laurie J, Barenghi CF (2012) Vortex-density fluctuations, energy spectra, and vortical regions in superfluid turbulence. *Phys Rev Lett* 109:205304.
 - [35] Nemirovskii SK, Tsubota M, Araki T (2002) Energy spectrum of the random velocity field induced by a Gaussian vortex tangle in He II. *J Low Temp Phys* 126:1535.
 - [36] Barenghi CF, Gordeev AV, Skrbek L (2006) Depolarization of decaying counterflow turbulence in He II. *Phys Rev E* 74:026309.
 - [37] Tough JT (1982) Superfluid Turbulence, *Prog Low Temp Phys* 8:133.
 - [38] Chagovets TV, Skrbek L (2008) Steady and decaying flow of He II in a channel with ends blocked by superleaks. *Phys Rev Lett* 100:215302.
 - [39] Salort J, Chabaud B, L  v  que E, Roche P-E (2011) Energy cascade and the four-fifths law in superfluid turbulence. *Europhys Lett* 97:34006.
 - [40] Araki T, Tsubota T, Nemirovskii SK (2002) Energy spectrum of superfluid turbulence with no normal-fluid component. *Phys Rev Lett* 89:145301.
 - [41] Morris K, Koplik J, Rouson D (2008) Vortex locking in direct numerical simulations of quantum turbulence. *Phys Rev Lett* 101:015301.
 - [42] Kivotides D (2006) Coherent structure formation in turbulent thermal superfluids. *Phys Rev Lett* 96:175301.
 - [43] Farge M, Schneider K, Pellegrino G, Wray AA, Rogallo RS (2003) Coherent vortex extraction in three-dimensional homogeneous turbulence: Comparison between CVS-wavelet and POD-Fourier decompositions. *Phys Fluids* 15:2886-2896.
 - [44] Walmsley PM, Golov AI (2008) Quantum and quasi-classical types of superfluid turbulence. *Phys Rev Lett* 100:245301.
 - [45] Bradley DI et al. (2006) Decay of pure quantum turbulence in superfluid $^3\text{He-B}$. *Phys Rev Lett* 96:035301.
 - [46] Fujiyama S et al. (2010) Generation, evolution and decay of pure quantum turbulence: a full Biot-Savart simulation. *Phys Rev B* 81:180512(R).
 - [47] Baggaley AW, Barenghi CF, Sergeev YA (2012) Quasiclassical and ultraquantum decay of superfluid turbulence. *Phys Rev B* 85:060501.
 - [48] Aarts RGKM, and de Waele ATAM (1994) Numerical investigation of the flow properties of He II. *Phys Rev B* 50:10069-10079.
 - [49] Finne AP et al. (2003) An intrinsic velocity-independent criterion for superfluid turbulence. *Nature* 424:1022-1025.
 - [50] Eltsov VB et al. (2009), Turbulent dynamics in rotating helium superfluids. *Prog Low Temp Phys* 16:45-146.
 - [51] Finne AP et al. (2006) Vortex multiplication in applied flow: a precursor to superfluid turbulence. *Phys Rev Lett* 96:085301.
 - [52] de Graaf R et al. (2008) The dynamics of vortex generation in superfluid $^3\text{He-B}$. *J Low Temp Phys* 153:197-227.
 - [53] Eltsov VB et al. (2010) Vortex formation and annihilation in rotating superfluid $^3\text{He-B}$ at low temperatures. *J Low Temp Phys* 161:474-508.
 - [54] Blaauwgeers R et al. (2002) Shear flow and Kelvin-Helmholtz instability in superfluids. *Phys Rev Lett* 89:155301.
 - [55] Eltsov VB et al. (2006) Twisted vortex state. *Phys Rev Lett* 96:215302.
 - [56] Eltsov VB et al. (2007) Quantum turbulence in a propagating superfluid vortex front. *Phys Rev Lett* 99:265301.
 - [57] Hosio JJ et al. (2011) Superfluid vortex front at $T \rightarrow 0$: Decoupling from the reference frame. *Phys Rev Lett* 107:135302.
 - [58] Hosio JJ et al. (2013) Energy and angular momentum balance in wall-bounded quantum turbulence at very low temperatures. *Nat Comm* 4:1614.
 - [59] Silaev MA (2012) Universal mechanism of dissipation in Fermi superfluids at ultralow temperatures. *Phys Rev Lett* 108:045303.
 - [60] H  nninen R (2009) Rotating inclined cylinder and the effect of the tilt angle on vortices. *J Low Temp Phys* 156:145-162.
 - [61] Walmsley PM, Golov AI, Hall HE, Levchenko AA, Vinen WF (2007) Dissipation of quantum turbulence in the zero temperature limit. *Phys Rev Lett* 99:265302.
 - [62] Eltsov VB et al. (2010) Stability and dissipation of laminar vortex flow in superfluid $^3\text{He-B}$. *Phys Rev Lett* 105:125301.
 - [63] Sonin EB (1987) Vortex oscillations and hydrodynamics in rotating superfluids. *Rev Mod Phys* 59:87-155.
 - [64] H  nninen R, Tsubota M, and Vinen WF (2007) Generation of turbulence by oscillating structures in superfluid helium at very low temperatures. *Phys Rev B* 75:064502.
 - [65] Skrbek L, Vinen WF (2009) The use of vibrating structures in the study of quantum turbulence. *Prog Low Temp Phys* 16:195-246.
 - [66] Nakatsuji A, Tsubota M, and Yano H (2013) Propagation of quantized vortices driven by an oscillating sphere in superfluid ^4He . *J Low Temp Phys* 171:519-525.
 - [67] Goto R et al. (2008) Turbulence in boundary flow of superfluid ^4He triggered by free vortex rings. *Phys Rev Lett* 100:045301.
 - [68] Adrian RJ (1991) Particle-Imaging techniques for experimental fluid mechanics. *Ann Rev of Fluid Mech* 23:261-304.
 - [69] Grant I (1997) Particle image velocimetry: a review. *Proc Inst Mech Eng C* 211:55-76.
 - [70] Zhang T, Van Sciver SW (2005) Large-scale turbulent flow around a cylinder in counterflow superfluid ^4He (He(II)). *Nature Physics* 1:36-38.
 - [71] Bewley GP, Lathrop DP, Sreenivasan KR (2006) Visualization of quantized vortices. *Nature* 441:588.
 - [72] Poole DR, Barenghi CF, Sergeev YA, Vinen WF (2005) Motion of tracer particles in He II. *Phys Rev B* 71:064514.
 - [73] Kivotides D, Barenghi CF, Sergeev YA (2006) Numerical calculation of the interaction of superfluid vortices and a rigid sphere. *J Low Temp Phys* 144:121-134.
 - [74] Rubinow S I and Keller J B (1971) Force on a rigid sphere in an incompressible inviscid fluid. *Phys Fluids*

- 14:1302-1304.
- [75] Schwarz KW (1974) Spherical probes and quantized vortices: Hydrodynamic formalism and simple applications. *Phys Rev A* 10:2306-2317.
 - [76] Kivotides D, Barenghi CF, Mee AJ, Sergeev YA (2007) Interactions of solid particles with a tangle of vortex filament in a viscous fluid. *Phys Rev Lett* 99:074501.
 - [77] Kivotides D, Barenghi CF, Sergeev YA (2007) Collision of a tracer particle and a quantized vortex in superfluid helium: Self-consistent calculations. *Phys Rev B* 75:212502.
 - [78] Kivotides D, Barenghi CF, Sergeev YA (2008) Interactions between particles and quantized vortices in superfluid helium. *Phys Rev B* 77:014527.
 - [79] Kivotides D, Sergeev YA, Barenghi CF (2008) Dynamics of solid particles in a tangle of superfluid vortices at low temperatures. *Phys Fluids* 20:055105.
 - [80] Paoletti MS, Fisher ME, Sreenivasan KR, Lathrop DP (2008) Velocity statistics distinguish quantum turbulence from classical turbulence. *Phys Rev Lett* 101:154501.
 - [81] White AC, Barenghi CF, Proukakis NP, Youd AJ, Wacks DH (2010) Nonclassical velocity statistics in a turbulent atomic Bose-Einstein condensate. *Phys Rev Lett* 104:075301.
 - [82] Adachi H, Tsubota M (2011) Numerical study of velocity statistics in steady counterflow quantum turbulence. *Phys Rev B* 83:132503.
 - [83] Salort J, Chabaud B, L  v  que E, Roche P-E (2012) Energy cascade and the four-fifths law in superfluid turbulence. *Europhys Lett* 97:34006.
 - [84] Baggaley AW, Barenghi CF (2011) Quantum turbulent velocity statistics and quasiclassical limit. *Phys Rev E* 84:067301.
 - [85] J  ger J, Schuderer B, Schoepe W (1995) Turbulent and laminar drag of superfluid helium on an oscillating microsphere. *Phys Rev Lett* 74:566-569.
 - [86] Bradley DI (2000) Repetitive single vortex-Loop creation by a vibrating wire in superfluid $^3\text{He-B}$. *Phys Rev Lett* 84:1252-1255.
 - [87] Schoepe W (2004) Fluctuations and stability of superfluid turbulence at mK temperatures. *Phys Rev Lett* 92:095301.
 - [88] Bradley DI et al. (2013) The onset of vortex production by a vibrating wire in superfluid $^3\text{He-B}$. *J Low Temp Phys* 171:582-588.
 - [89] Thomson W (1880) Vibrations of a columnar vortex. *Phil Mag* 10:155-168.
 - [90] Bradley DI et al. (2006) Decay of pure quantum turbulence in superfluid $^3\text{He-B}$. *Phys Rev Lett* 96:035301.
 - [91] Kivotides D, Vassilicos JC, Samuels DC, and Barenghi CF (2001) Kelvin wave cascade in superfluid turbulence. *Phys Rev Lett* 86:3080.
 - [92] Nazarenko SV (2011) Wave Turbulence (Springer).
 - [93] Kozik E, Svistunov B (2004) Kelvin wave cascade and decay of superfluid turbulence. *Phys Rev Lett* 92:035301.
 - [94] L'vov VS, Nazarenko S (2010) Spectrum of Kelvin-wave turbulence in superfluids. *JETP Lett* 91:428-434.
 - [95] Sonin EB (2012) Symmetry of Kelvin-wave dynamics and the Kelvin-wave cascade in the $T = 0$ superfluid turbulence. *Phys Rev B* 85:104516.
 - [96] Vinen WF, Tsubota M, Mitani A (2003) Kelvin-wave cascade on a vortex in superfluid ^4He at a very low temperature. *Phys Rev Lett* 91:135301.
 - [97] Kozik E, Svistunov B (2005) Scale-separation scheme for simulating superfluid turbulence: Kelvin-wave cascade. *Phys Rev Lett* 94:025301.
 - [98] Baggaley AW, Barenghi CF (2011) Spectrum of turbulent Kelvin-waves cascade in superfluid helium. *Phys Rev B* 83:134509.
 - [99] H  nninen R, Hietala N (2013) Identification of Kelvin waves: numerical challenges. *J Low Temp Phys* 171:485-496.
 - [100] Kozik E, Svistunov B (2008) Kolmogorov and Kelvin-wave cascades of superfluid turbulence at $T = 0$: what lies between. *Phys Rev B* 77, 060502(R).
 - [101] Kursu M, Bajaj K, Lipniacki T (2011) Cascade of vortex loops initiated by a single reconnection of quantum vortices. *Phys Rev B* 83:014515.
 - [102] Andersson N, Glampedakis K, Ho WCG, Espinoza CM (2012) Pulsar glitches: the crust is not enough. *Phys Rev Lett* 109:241103.